HHS Public Access

Author manuscript

Nat Genet. Author manuscript; available in PMC 2012 October 01.

Published in final edited form as:

Nat Genet. ; 44(4): 381–S2. doi:10.1038/ng.1106.

Mutations in axonemal dynein assembly factor *DNAAF3* cause primary ciliary dyskinesia

Hannah M. Mitchison[1,*], **Miriam Schmidts**[1], **Niki T. Loges**[2], **Judy Freshour**[3], **Athina Dritsoula**[1], **Rob A. Hirst**[4], **Christopher O'Callaghan**[4], **Hannah Blau**[5], **Maha Al Dabbagh**[6], **Heike Olbrich**[2], **Philip L. Beales**[1], **Toshiki Yagi**[7], **Huda Mussaffi**[5], **Eddie M.K. Chung**[8], **Heymut Omran**[2], and **David R. Mitchell**[3,*]

[1]Molecular Medicine Unit, University College London Institute of Child Health, London, UK

[2]Department of Pediatrics and Adolescent Medicine, University Hospital Muenster, Germany

[3]Cell and Developmental Biology, SUNY Upstate Medical University, Syracuse, NY, USA

[4]Department of Infection Immunity and Inflammation, University of Leicester, Leicester Royal Infirmary, Leicester, UK

[5]Pulmonary Unit, Schneider Children's Medical Center of Israel, Petah-Tikva, Sackler School of Medicine, Tel-Aviv University, Tel-Aviv, Israel

[6]Department of Pulmonary Section, Department of Pediatrics, King Fahd Armed Forces Hospital, Jeddah, Saudi Arabia

[7]Department of Cell Biology and Anatomy, Graduate School of Medicine, University of Tokyo, Tokyo, Japan

[8]General and Adolescent Paediatric Unit, University College London Institute of Child Health, London, UK

Abstract

Primary Ciliary Dyskinesia (PCD) most often arises from loss of the dynein motors that power ciliary beating. Here we show that PF22/DNAAF3, a previously uncharacterized protein, is essential for the preassembly of dyneins into complexes prior to their transport into cilia. We

[*]Correspondence: David R. Mitchell, Cell and Developmental Biology, 1133 WH, SUNY Upstate Medical University, 750 E. Adams St., Syracuse, NY 13210, Tel: 1-315-464-8575, Fax: 1-315-464-8535, mitcheld@upstate.edu, Hannah M. Mitchison, Molecular Medicine Unit, University College London (UCL) Institute of Child Health, 30 Guilford Street, London, WC1N 1EH, UK, Tel: 44-20-7905-2866, Fax: 44-20-7404-6191, h.mitchison@ucl.ac.uk.

Accession numbers

The *Chlamydomonas DAB1* gene sequence appears in Genbank as HQ424432 and the corresponding PF22 protein sequence as AEC04845.

Author Contributions

Studies on human samples were conducted by H.M.M., A.D., H.B., N.T.L., M.A.D., H. Olbrich, H.M., E.M.K.C., and H. Omran. Studies in *Chlamydomonas* were designed by D.R.M. and carried out by D.R.M. and J. F.; T.Y. contributed essential reagents and data analysis. Studies in zebrafish were designed by H.M.M. and conducted by H.M.M., M.S., A.D., R.A.H., C.O. and P.L.B. The manuscript was written by D.R.M. and H.M.M.

Competing Financial Interests

The authors declare that they have no competing financial interests related to this publication.

identified loss-of-function mutations in the human *DNAAF3* gene in patients from families with *situs inversus* and defects in assembly of inner and outer dynein arms. Zebrafish *dnaaf3* knockdown likewise disrupts dynein arm assembly and ciliary motility, causing PCD phenotypes including hydrocephalus and laterality malformations. *Chlamydomonas reinhardtii* PF22 is exclusively cytoplasmic, and a null mutant fails to assemble outer and some inner dynein arms. Altered abundance of dynein subunits in mutant cytoplasm suggests PF22/DNAAF3 acts at a similar stage to other preassembly proteins, PF13/KTU and ODA7/LRRC50, in the dynein preassembly pathway. These results support the existence of a conserved multi-step pathway for cytoplasmic formation of assembly-competent ciliary dynein complexes.

Keywords

Kartagener syndrome; primary ciliary dyskinesia; *Chlamydomonas*; flagella; dynein assembly; zebrafish

PCD (MIM 244400) affects 1:15-30,000 live births and arises from ultrastructural defects causing dysmotility of motile cilia/flagella in the respiratory epithelia, brain ependyma, embryonic node, oviduct and sperm. Ineffective airway mucociliary clearance usually manifests within the first year of life with recurrent infections, sinusitis, rhinitis and otitis media, causing a chronic respiratory condition, and progressing to permanent lung damage (bronchiectasis)[1,2]. Half of PCD patients have laterality defects reflecting randomized left-right organogenesis due to embryonic nodal cilia dysfunction, usually *situs inversus totalis* (Kartagener syndrome) with rarer incidence of complex heterotaxy defects often associated with congenital heart disease[3,4, 5]. Subfertility arises from dysmotile sperm flagella and oviduct cilia, and hydrocephalus occasionally arises [6] from reduced cerebrospinal fluid flow due to ependymal cilia dysmotility[7,8].

The core '9+2' ciliary axoneme consists of nine peripheral outer doublet microtubules surrounding a central microtubule pair. Additional components along each doublet include inner and outer dynein arms that hydrolyze ATP to power ciliary movement, radial spokes that modulate ciliary beating[9,10], and a spoke-associated dynein regulatory complex[11]. PCD is usually autosomal recessive and is genetically heterogeneous due to a range of ultrastructural ciliary axoneme defects, >70% involving loss of outer dynein arms[12,13]. Disease-causing mutations have been identified in thirteen genes including five encoding outer dynein arm subunits (*DNAH5*[14], *DNAH11*[15], *DNAI1*[16], *DNAI2*[17], *DNAL1*[18], *TXNDC3*[19]) and two unique dynein assembly loci, *DNAAF1*[20] and *DNAAF2*[21,22] (dynein, axonemal, assembly factor 1 (*DNAAF1; KTU; PF13*) and 2 (*DNAAF2; LRRC50; ODA7)*). Null-mutant strains of the biflagellate alga *Chlamydomonas reinhardtii* lacking DNAAF1 and DNAAF2 orthologous proteins (PF13 and ODA7 respectively) are deficient for pre-assembly of dynein arm complexes in the cytoplasm. Patients carrying *DNAAF1* and *DNAAF2* mutations are deficient in inner as well as outer dynein arm assembly. Here we describe DNAAF3/PF22, a new cytoplasmic factor needed for assembly of axonemal inner and outer dynein arms.

Results

PF22 defines a new axonemal dynein assembly locus

Most *Chlamydomonas* outer dynein arm (ODA) assembly mutants swim slowly with a reduced beat frequency, but flagella remain full length[23]. The *Chlamydomonas pf22* strain was previously shown to be non-motile, with paralyzed half-length flagella and disrupted ODA assembly[24]. At least two inner dynein arm (IDA) components were also reduced or missing[25,26]. We further analyzed dynein assembly in *pf22* because it resembles *pf13,* a mutant lacking a conserved dynein assembly factor that has been implicated in a chaperoning step of dynein assembly[20]. Blots of demembranated flagellar axonemes (Fig. 1a) confirm that ODA assembly is greatly reduced in *pf22*, seen as a general reduction in dynein heavy chains (DHCs) and specific loss of IC2, a dynein intermediate chain (DIC) essential for ODA assembly in *Chlamydomonas* and humans[17,27]. In addition to ODAs, *Chlamydomonas* flagella contain at least seven major IDAs, designated "a-g"[28]. IDA dyneins "b" (DHC5) and "c" (DHC9) fail to assemble in *pf22* axonemes, whereas dimeric IDA dynein "f" (DIC140) is retained (Fig. 1a). This pattern resembles that of *pf13*, which also lacks ODA dyneins and IDA dynein "c", but not "f"[20]. In contrast, loss of cytoplasmic factor ODA7 disrupts ODA but not IDA assembly in *Chlamydomonas*[29].

We identified the gene disrupted by the *pf22* mutation through molecular mapping and phenotypic rescue (see Methods and Supplementary Fig. 1 for cloning details). Transforming a 7.2 kb genomic fragment spanning a single gene rescued the *pf22* phenotype (short flagella, lack of motility and dynein assembly defect) to wild-type (Fig. 1a, lane 3). This gene is formally designated Dynein Assembly Blocked 1 (*DAB1*) to conform with a recently adopted *Chlamydomonas* dynein-associated gene nomenclature[30]. The predicted 710 amino acid *Chlamydomonas* PF22 protein (molecular weight 72,731 Da), contains no characterized structural motifs or similarity to known proteins. A single homolog could be identified in the genomes of most organisms with motile cilia or flagella, but not those lacking cilia or only retaining non-motile sensory cilia (e.g., *C. elegans*). An overall pattern of sequence evolution roughly parallel to that of eukaryotic organisms suggests that PF22 performs an evolutionarily conserved function in axonemal dynein assembly (Fig. 1b and Supplementary Fig. 2). The *Chlamydomonas* and human ortholog sequences are similar over their entire lengths except for two insertions in the C-terminal half of the algal protein (Fig. 1c). The *Chlamydomonas pf22* mutant *DAB1* gene has a single G to A base change in exon 3 at codon 79, TGG -> TGA, altering a tryptophan to a nonsense codon (p.Trp79X) and predicting a null allele due to early termination of the PF22 protein after 78 out of 710 residues.

PF22 functions in the cytoplasm

Chlamydomonas mutant strains that do not assemble ODA complexes can carry mutations in dynein subunits[31], in dynein-specific transport factors[32] and in cytoplasmic assembly proteins[20,21,33]. To reveal its normal role in dynein assembly, we expressed an N-terminal cMyc epitope tagged PF22 protein in *pf22* mutant cells, which fully complemented the mutant motility phenotype (Supplementary Movies 1-3) and rescued flagellar assembly of ODAs (IC2), and IDAs (DHC5 and DHC9) (Fig. 1a, lane 4). Cell fractionation showed that

the MycPF22 protein migrates as a 60 kDa band in cytoplasmic fractions, whereas no equivalent band was seen in axonemal fractions even when loaded at a 50X stoichiometric excess (Fig. 1d). In contrast, dynein subunits such as IC2 (Fig. 1d) and transport factors such as ODA16[32,34] are present in both the cytoplasm and flagella. PF22 therefore displays properties consistent with a role in forming axonemal dyneins into assembly-competent complexes in the cytoplasm, prior to their intraflagellar transport-mediated movement into flagella. Immunoprecipitation of tagged PF22 protein failed to co-precipitate outer dynein arm subunits or other known dynein assembly factors, suggesting any such interactions may occur only transiently during dynein complex formation (not shown).

Mutations in the human *PF22* (*DNAAF3*) gene cause PCD

The human *DAB1* orthologous gene *DNAAF3* on human chromosome 19q13 (previously designated *C19orf51*) encodes a 588 amino acid protein (Genbank NP_849159). It was identified in expression studies as a potential cilia-related gene[35] whose transcript abundance increased 5.62-fold during cilia formation[36]. The *DNAAF3* gene resides within a previously described PCD locus (*CILD2* locus; MIM 606763) mapped in consanguineous Arabic-origin PCD families characterized by immotile cilia with absent ciliary outer arm dyneins[37]. We detected homozygous mutations in *DNAAF3* in two of the three originally linked families (UCL66/67 and UCL89), both of which display large regions of marker homozygosity across the *DNAAF3* locus in affected individuals (Fig. 2a and Supplementary Table 1). Two different mutations were detected: c.323T>C in exon 3 creating missense mutation p.Leu108Pro in family UCL89, and c.406C>T in exon 4 creating nonsense mutation p.Arg136X in family UCL66/67 (Fig. 2b). Neither variant was present on 148 population-matched control Arabic chromosomes. The p.Leu108Pro mutation was predicted with 100% confidence to be 'probably damaging' using Polyphen2[38] and SIFT[39], and is highly conserved across ciliated species (Fig. 2c).

We sequenced *DNAAF3* in 112 additional PCD families, 107 with outer dynein arm defects and 9 with evidence for linkage to the chromosome 19 locus. Of these, one family showing evidence of linkage (UCL71, Fig. 2a) had a homozygous single basepair insertion within *DNAAF3* exon 6, c.762_763insT, creating a predicted frameshift that generates 11 novel amino acids after a p.Val255Cys change followed by a premature stop codon (p.Val255CysfsX12) (Fig. 2a, b). UCL71 is a first-cousin union UK-Pakistani family and this variant was absent from172 control UK-Pakistani chromosomes. An additional homozygous single basepair substitution (c.973G>A) identified in a Belgian patient (OP-549) creates a missense variant, p.Ala325Thr. However, one of 192 Caucasian control chromosomes carried this variant, which is predicted as 'benign' using Polyphen2 and SIFT. This residue is not conserved and this variant is likely to be a Caucasian polymorphism.

For p.Leu108Pro, p.Arg136X and p.Val255CysfsX12, all affected individuals carried homozygous mutations while unaffected parents and siblings carried heterozygous changes consistent with recessive inheritance (Fig. 2a, Supplementary Table 1). None of these mutations are present in the dbSNP, 1000 Genomes or NHLBI-ESP polymorphism databases. Supplementary Table 2 contains detailed clinical information for these three families.

PCD patients with *DNAAF3* mutations have axonemal dynein arm assembly defects

Respiratory cells obtained by nasal-brushing biopsy from *DNAAF3* patients were analyzed for expression of ODA proteins DNAH5, DNAH9, DNAI2 (orthologs of *Chlamydomonas* dynein DHCs γ and β and DIC IC2 respectively) and IDA component DNALI1 (*Chlamydomonas* p28) using antibodies against these human outer and inner dynein arm components. We previously showed that respiratory cilia contain two distinct ODA types: type 1, DNAH9-negative and DNAH5-positive (proximal ciliary axoneme); and type 2: DNAH9- and DNAH5-positive (distal ciliary axoneme)[40]. ODA components DNAH5 (Fig. 3), DNAH9 and DNAI2 (see Supplementary Fig. 3 and 4), and IDA light chain DNALI1 (Fig. 4) were all absent from the cilia of affected patients. These results suggest that DNAAF3 is important for the assembly of outer and inner dynein arms along the entire length of the axoneme, comprising ODA types 1 and 2 and the DNALI1 containing IDA types. Electron microscopy confirmed an abnormal ultrastructure missing ODAs and IDAs (Fig. 3a). Furthermore, cilia in nasal brushing biopsies were immotile in all affected family members (Supplementary table 2).

Knockdown of zebrafish *dnaaf3* affects motile cilia in multiple tissue types

We determined the effects of dnaaf3 loss during zebrafish development by gene silencing, using antisense morpholinos directed against the 5'UTR to block protein translation, and against the exon 3-intron 3 (*dnaaf3* MO ex3) and exon 8-intron 8 (*dnaaf3* MO ex8) splice donor sites to block splicing (see Supplementary Fig. 5b for evidence of reduced expression). Injection of 2-8 ng of any of these morpholinos at the one-cell stage gave rise to similar dose-dependent phenotypes at 3 days post fertilization (dpf) including completely static olfactory placode cilia, as illustrated by high speed video microscopy, recapitulating the immotile nasal cilia in PCD *DNAAF3* patients; reduced movement of debris in the olfactory placode further indicated a lack of fluid flow (Supplementary Movies 4, 5). The morphology and number of cilia in the olfactory placode of morphant fish was unaffected, but electron microscopy revealed abnormal ultrastructure including reduced or missing ODAs and IDAs (Fig. 5).

Several cilia-related phenotypes were seen at 3 dpf in morphant fish, with *dnaaf3*^{MOex8} morphants most severely affected. Abnormal body axis curvature, with the downward-curving tail (Fig. 5a, b) typical of zebrafish with defects in cilia motility [41-43] or assembly [44] was observed in 64% of *dnaaf3*^{MOex3} and 78% of *dnaaf3*^{MOex8} embryos. Hydrocephalus was also present in 18% of *dnaaf3*^{MOex3} and 34% of *dnaaf3*^{MOex8} embryos (Fig. 5c-e, asterisks). Pronephric cysts developed progressively in *dnaaf3*^{MOex8} embryos from 2 dpf (49%) to 5 dpf (77%) (Fig. 5 a-d, arrows). The pronephric cilia of 3 dpf *dnaaf3*^{MOex8} embryos had a reduced and disorganized beat frequency (not shown), as did spinal cord cilia (Supplementary Movies 6, 7). Normal otolith assembly and localization (required for gravitaxis and balance) depends on motile tether cilia within the otic vesicle [45]. While control embryos invariably had two otoliths, 27% of *dnaaf3*^{MOex8} embryos had 1-3 otoliths, which often appeared malformed (Fig. 5e; see also Supplementary Fig. 5a). Like PCD patients, the morphant zebrafish embryos displayed perturbed left-right axis patterning, with about half of *dnaaf3*^{MOex8} embryos exhibiting either reversed or no heart looping (Fig. 5g).

By in situ hybridization, *dnaaf3* was most strongly expressed in cell types that express axonemal dyneins (see Supplementary Fig. 5c), similar to the patterns shown previously for *dnaaf2*[42].

Loss of PF22/DNAAF3 affects a similar stage of cytoplasmic assembly to PF13/DNAAF1 and ODA7/DNAAF2

More direct biochemical analyses of the mechanism of PF22 action relied upon the cytoplasmic pool of axonemal proteins (including dynein subunits) that accumulates in *Chlamydomonas.* This pool is large enough to support the assembly of half-length flagella in the absence of protein synthesis[46]. Loss of function of the previously-characterized assembly factors PF13 and ODA7 increases the abundance of outer arm DIC subunits in this pool, but reduces the abundance of some DHC subunits. Blots of cytoplasmic extracts showed that in *pf22* cytoplasm ODA heavy chains HCα (no human ortholog), HCβ (orthologous to human DNAH9, DNAH11 and DNAH17) and HCγ (orthologous to human DNAH5, DNAH8) are all retained at nearly wild type levels, whereas ODA intermediate chain IC2 (human DNAI2) is hyper-abundant (Fig. 6a; see Supplementary Fig. 6 for densitometric quantification of DHCs in all panels of Fig. 6). Both *oda7* and *pf13* display a similar ca. 7-fold increase in cytoplasmic IC2 abundance, but substantial reductions in HCβ and HCγ, and *oda7* shows almost a complete loss of HCα. Thus, *pf22* is similar to these previously-characterized mutants in its affect on intermediate chain abundance, suggesting a similar defect in assembling heavy chains with intermediate chains. However *pf22* does not substantially alter heavy chain abundance, suggesting it may work at a different step in the assembly process.

To see if *pf22* functions upstream or downstream of *oda7* in a linear pathway, the abundance of HCα was compared in extracts of wild type, *pf22*, *oda7*, and a *pf22oda7* double mutant strain. We reasoned that if *oda7* was upstream of *pf22*, then HCα abundance would be reduced to a similar level in *oda7* and the double mutant, whereas if *oda7* functioned downstream of *pf22*, then HCα might be protected from the effects of *oda7* in the double mutant strain. HCα abundance in the *pf22oda7* double mutant was intermediate between the levels in each individual mutant, arguing against a simple sequential pathway (Fig. 6b).

The improper assembly of dynein chains in mutant cytoplasm suggests a defect in a chaperone-dependent assembly step, consistent with the homology between *Chlamydomonas* dynein assembly proteins PF13 and MOT48, and yeast PIH1, a subunit of the HSP90-associated R2TP complex[20,33,47]. The globular motor domains of myosins require chaperones for normal folding[48], and we reasoned that *pf22* dynein assembly defects might also result from improper chaperone-dependent heavy chain folding. Trypsin-sensitivity assays were used to examine the folding state of dynein heavy chains in the cytoplasm of *Chlamydomonas* assembly mutants. Because the lack of association of heavy chains with intermediate chains could directly alter trypsin sensitivity, as a control we used cytoplasmic extracts from the *oda9* strain deficient for ODA intermediate chain IC1 (human DNAI1)[49]. *oda9* prevents ODA heavy chains from interacting in complexes but does not affect the abundance of these heavy chains[31], which remain fully competent for assembly,

based on full recovery of beat frequency in temporary diploids (dikaryons) formed by crossing *oda9* and the HCβ mutant *oda4*[23].

HCα showed altered trypsin-sensitivity in the *oda7* cytoplasm compared to control (*oda9*) cytoplasm, whereas neither *pf13* nor *pf22* alter the pattern of HCα trypsin sensitivity (Fig. 6c-e). This heightened trypsin sensitivity is apparent from a major band at about 200 kDa that is absent from the other strains (Fig. 6c, arrow), and the complete loss of a major high molecular weight tryptic fragment at 10 μg/ml trypsin (Fig. 6c, arrowhead). The antibody used for HCα recognizes N-terminal residues 512-838 of this 4499 residue heavy chain[31]. The new tryptic fragment generated in *oda7* extracts represents a hypersensitive site far from the N-terminus, in the dynein globular head domain. HCβ and HCγ both show increased sensitivity to tryptic proteolysis in all three mutant extracts, as seen by more rapid loss of full length heavy chain and by the appearance of new fragments (Fig. 6d, e; densitometric quantification in Supplementary Fig. 6). The HCβ antibody also recognizes an N-terminal tail domain epitope (residues 1129-1161 of this 4568 residue protein)[50], thus the HCβ hypersensitive site that gives rise to an approximately 300 kDa band in the *pf13* and *oda7* extracts (Fig. 6d) must also represent a site in the dynein catalytic head. Therefore both PF13 and ODA7 proteins may function in chaperoning steps that aid folding of DHCs. Heavy chain tryptic sensitivity is less strongly altered in *pf22*, and the pattern of sites sensitive to digestion did not change, therefore if PF22 acts as a co-chaperone, it likely works at a later step than PF13 and ODA7 such as the stabilization of heavy chains or the joining of heavy chains and smaller subunits into a larger complex, rather than folding of globular head domains.

Overall, the increase in proteolytic sensitivity of ODA heavy chains (Fig. 6c-e) appears to correlate with a decrease in their cytoplasmic abundance (Fig. 6a) suggesting that depletion of these heavy chains in mutant cytoplasm results from higher rates of degradation. To test this idea, we examined turnover rates by blocking protein synthesis with cycloheximide and blotting with dynein heavy chain-specific antibodies. Whole *pf22* cells were compared with the *pf13* and *oda7* strains known to block assembly in the cytoplasm, and with two strains that assemble normal ODA complexes in the cytoplasm, but block ODA assembly at later stages. These are *oda16,* in which ODA transport into flagella is blocked[32], and *oda1*, in which a dynein docking complex is prevented from binding to axonemal doublet microtubules[51]. HCα half-life exceeded 12 h in the *oda16* and *pf22* cytoplasm, but was shortened to about 8 h in *pf13* cytoplasm (Fig. 6f and Supplementary Fig. 6). Similarly, compared to o*da16* as a control, HCβ half-life was substantially reduced in *pf13* (ca. 5 h) and marginally reduced in *pf22* (ca. 12 h). The greatly reduced abundance of HCα in the *oda7* cytoplasm (Fig. 6a) correlates with a greatly reduced HCα half life, from over 24 h in *oda16* to less than 2 h in *oda7*; no difference in HCβ half life could be seen between *oda1* and *oda7*. We conclude that the reduced abundance of DHCs in these mutant strains is due to their increased rate of degradation. This could account for the disproportionate accumulation of IC2 if continued synthesis and turnover of heavy chains is accompanied by continued synthesis of intermediate chains without turnover.

To see if ODA heavy chain and intermediate chain association in the cytoplasm is disrupted in *pf22* we immunoprecipitated HCβ with a monoclonal antibody and blotted for the

presence of other ODA subunits. We previously showed that intact dynein complexes precipitate from wild-type cytoplasm, but only HCβ precipitates from *pf13*[20] or *oda7*[31] cytoplasm with this antibody. Surprisingly, no antigen was precipitated from *pf22* cytoplasm (Fig. 7a), even though near-normal levels of HCβ antigen were present in the *pf22* extracts (Fig. 6a). This result could be explained if the precipitating monoclonal antibody binding site is blocked by interaction with some other protein. As an alternative method to look for complexes, we tagged IC2 with an HA epitope near its N-terminus[52] and expressed it in the *oda6* strain, which has a frameshift mutation early in the IC2 gene[27]. The HA-IC2 protein supports normal dynein assembly[52] and can be used to immunoprecipitate an intact outer dynein arm complex (Fig. 7b). When HA-IC2 was immunoprecipitated from *pf22* cytoplasm, normal amounts of HCα and HCβ and reduced amounts of HCγ co-precipitated (Fig. 7b). This reduction in HCγ suggests that PF22-dependent chaperone activity may be important for correct association of HCs and ICs. Taken together, these results show that complexes can form in the *pf22* cytoplasm, but an epitope on the HCβ tail that is normally exposed is buried as a consequence of the loss of PF22 function, and the complexes that have formed cannot go on to assemble into flagella.

Discussion

Ciliary motility provides essential developmental signals for embryonic left-right pattern determination, and serves as a first means of defense against airborne pathogens. Although most PCD patients have defects in assembly of axonemal dyneins, many show no defects in any of the previously-identified candidate dynein assembly genes. Here we have identified mutations in the *DNAAF3* gene in PCD patients with immotile cilia that lack both outer and inner dynein arms. This new locus broadens the significance of cytoplasmic pre-assembly steps in the formation of axonemal dyneins and suggests that additional genes involved in this process should be tested as PCD candidates.

Based on the *Chlamydomonas* results presented here, cytoplasmic assembly of axonemal dynein motors requires at least two steps, an earlier step required for DHC stability that may involve folding of globular dynein head domains, and a later step that generates an assembly-competent complex between DHCs and smaller subunits (Fig. 8). Protease sensitivity assays support the role of PF13/DNAAF1 and ODA7/DNAAF2 in the earlier, DHC folding step but fewer abnormalities in folding were observed in *pf22*, suggesting that the failure in *pf22* occurs at a later step in the dynein assembly process. Immunoprecipitation shows that at least one heavy chain epitope exposed in wild type cytoplasm is inaccessible in the *pf22* cytoplasm, consistent with accumulation of an abnormal complex in the absence of PF22. We hypothesize that chaperones important for DHC folding and complex formation (Fig. 8, labeled with "?") depend on PF13, ODA7 and PF22 for substrate recognition, and on PF22 for product release. Based on the PIH domain in PF13, one likely candidate for a PF13-associated chaperone complex is the R2TP-prefoldin complex which, along with HSP90, has been implicated in assembly of many essential cellular complexes[53,54]. The *Chlamydomonas* motility-deficient strain *ida10* has a mutation in *MOT48*, a paralog of *PF13*[33]. The loss of *MOT48* only affects assembly of a subset of IDAs, but as in *pf13*, an affected DHC in *ida10* failed to co-precipitate with a smaller subunit, and its abundance in the cytoplasm was decreased. Thus factors important for early steps in DHC folding/stability

and for their successful association with other subunits, may be required for all axonemal dyneins. Inability of the ODA complex that accumulates in the *pf22* cytoplasm to assemble into flagella and form functional dynein arms could reflect a defect in the interaction of the ODA complex with either the IFT transport machinery, or with binding sites on the axoneme's peripheral doublet microtubules.

The evolutionarily conserved role of PF22 in this pathway is evident in the similar phenotypes seen in the algal mutant, zebrafish knockdowns, and human patients. Previous studies showed that flagella from *Chlamydomonas pf22* strains retain about 66% of wild type levels of p28, the algal ortholog of IDA subunit DNALI1[25], whereas our immunofluorescent analysis shows that mutations in human *DNAAF3* completely block assembly of DNALI1. Thus either the pattern of p28 association with inner row dyneins, or the array of dyneins dependent on PF22/DNAAF3 for their assembly, has changed during the evolution of mammals and alga from a common ancestor. In some patients, residual DNAH5 and DNALI1 can be seen in the apical cytoplasm, whereas cytoplasmic accumulation of these proteins is not seen in control samples. A similar cytoplasmic accumulation of unassembled IC2 subunits in the *pf22* alga model suggests that assembly is blocked at a similar stage. In zebrafish, DNAAF3 knockdown also results in disrupted dynein assembly and loss of ciliary motility in several tissues, linked to the curly-tail, hydrocephalus, otolith, laterality and pronephric cyst phenotypes typical of motile cilia disorders[41,45] including those linked to genes needed for cytoplasmic pre-assembly of axonemal dyneins[20,42,55]. Left-right patterning defects in *dnaaf3* morphant embryos (Fig. 5) parallel the appearance of situs inversus in the human patient population[37] and confirm a role for DNAAF3 in assembly of dyneins critical for nodal cilia motility. Although we obtained no direct evidence for the localization of DNAAF3 in either fish or human tissues, only in *Chlamydomonas*, the similar phenotype resulting from its loss from vertebrates and *Chlamydomonas*, and the absence of this protein from any published proteomic studies of cilia or spermatozoa, supports the hypothesis that PF22/DNAAF3 functions exclusively in the cytoplasm.

In conclusion, we have shown an essential role for PF22/DNAAF3, a conserved dynein assembly factor unrelated to any previously-characterized proteins, in assembly of multiple ciliary axonemal dyneins. Its loss prevents correct assembly of inner and outer dynein arms, abolishing motility of respiratory cilia and giving rise to classical PCD associated with defective left-right organ asymmetry and male infertility. PF22/DNAAF3 function appears related to, but different from, that of other recently identified PCD proteins PF13/DNAAF1[20], ODA7/DNAAF2[21], and MOT48[33]. Together, these dynein assembly factors define a new multi-step pathway, required for cytoplasmic assembly of axonemal dyneins, that may involve proper folding of individual DHCs as well as their association into larger, multi-subunit complexes. Because cilia and flagella require many dynein isoforms for their normal function, and the assembly factors studied to date do not appear to be responsible for the formation of all of these axonemal dynein complexes, future studies may identify additional proteins involved in these cytoplasmic assembly steps.

Supplementary Material

Refer to Web version on PubMed Central for supplementary material.

Acknowledgements

We wish to express thanks to the patients and their families for their participation and to the physicians involved, particularly Dr Hamish Simpson, Dr Jane Clarke and Dr David Spencer. We are grateful to Mark Turmaine for zebrafish EM. Winfield Sale (Emory Univ) and Stephen King (Univ Conn) provided antibodies to *Chlamydomonas* dynein subunits. We thank R. Mark Gardiner, Sarah Spiden, Maggie Meeks, Dinu Antony and Daniel Osborn for advice and assistance. We also thank Angelina Heer, Denise Nergenau, Christina Reinhard, Carmen Kopp, Karin Sutter, Claudia Tessmer, Theresia de Ledezma, and Susanne Franz for excellent technical assistance. The work conducted by the U.S. Department of Energy Joint Genome Institute is supported by the Office of Science of the U.S. Department of Energy under Contract No. DE-AC02-05CH11231. DRM was supported by NIH grant R01-GM022448. HM received support from the PCD Family Support Group (UK) and funding from the Fondation Milena Carvajal Pro-Kartagener, the Medical Research Council UK, the Wellcome Trust and Action Medical Research. HO was supported by grants from the Deutsche Forschungsgemeinschaft (DFG) (Om 6/4, GRK1104, BIOSS, and SFB592).

Appendix

Methods

Families, clinical information and controls

Informed consent was obtained from patients and family members in accordance with protocols approved by the University College London Hospital NHS Trust ethical committee and collaborating institutions. The diagnosis of PCD was made according to standard clinical criteria. All the PCD families reported here presented with classic clinical symptoms that included neonatal respiratory distress, recurrent cough and wheezing, nasal discharge and chest infections, sinusitis, otitis media, nasal polyps and bronchiectasis.

Clinical features of the 10 patients carrying *DNAAF3* mutations are detailed in Supplementary Table 2. The families studied included Arabic origin consanguineous PCD pedigrees with a ciliary ultrastructural defect of absent dynein arms, previously reported to link to a common locus[37]. The parents of all affected individuals except UCL66/67 III.1 and III.2 are first cousins. Four out of the 10 affected individuals have *situs inversus* (Fig. 2). Electron microscopy of respiratory cilia for these families, where available, indicated a common defect involving reduced or absent inner and outer dynein arms (Fig. 3). The *DNAAF3* gene was sequenced in 112 additional PCD families that were consistent with linkage to this locus and/or had PCD with absent outer dynein arms confirmed either at the LM or EM level.

The control DNAs have been previously reported[10] and consisted of anonymized UK-Pakistani individuals, Bedouin samples purchased from the National Laboratory for the Genetics of Israeli populations (http://nlgip.tau.ac.il/), and additional unrelated members of other pedigrees (Pakistani and Arabic) collected for mapping/polymorphism studies. The Caucasian control DNAs consisted of UK-Northern European samples from the ECACC (http://www.ecacc.org.uk/) Human Random Control Collection.

Chlamydomonas strains and genetic analysis

Chlamydomonas strains included *arg7*, *oda1, oda6, oda7*, *oda9, oda16, pf13*, *pf22*, *S1D2*, and *137c* (wild type), and were obtained from the Chlamydomonas Center. For AFLP mapping of the *DAB1* locus, *pf22* was first back-crossed twice to wild type strain *137c*. 68 random products from a *pf22* × *S1D2* cross were tested for co-segregation of the mutant phenotype and the *137c* allele for markers on Chromosome 1, including ARG7 and CYP1[56], two markers on scaffold 96 and three markers on scaffold 53 of the JGI *Chlamydomonas* genome (http://genomeportal.jgi-psf.org/Chlre3/Chlre3.home.html). Based on the number of recombinants observed between *pf22* and each marker (9 for ARG7, 4 for CYP1, 2 for 96-200, 1 each for 96-120, 53-431, and 53-405, and 0 for 53-34), genomic clones from a BAC library that spanned the first 325 kb of scaffold 53 (PTQ9647, PTQ8519, PTQ968, PTQ14096 and PTQ6338) were co-transformed with an *ARG* gene plasmid into a *pf22arg7* strain. The genetic interval spanning *DAB1* was defined by the sequences unique to PTQ14096, the only BAC that rescued the paralyzed phenotype (see Supplementary Fig. 1 for details). Motility of *Chlamydomonas* was recorded on a Zeiss Axioskop with darkfield illumination through a 635 nm cutoff filter. Video images captured at 30 fps were analyzed using CellTrak 1.5 software (Motion Analysis Corp, Santa Rosa, CA) to determine swimming speeds.

Chlamydomonas gene cloning and epitope tag expression

Genomic sequences unique to BAC PTQ14096 encoded a predicted protein, similar to *Volvox carteri* protein ID 106739, that identified a gene conserved in organisms with motile cilia. A 10 kb *Sal I-Eco RI* fragment from BAC PTQ14096 was subcloned into pBIISK (+) to make plasmid pBPF22SE (Supplementary Fig. 1), and shown to retain the ability to rescue the *pf22* mutant phenotype. The intron-exon structure of the encoded *Chlamydomonas PF22* gene was predicted based on consensus *Chlamydomonas* splice junctions and on similarity of the translated exons to sequences of potential homologs from other sequenced genomes. Based on the location of predicted exons in this sequence, an additional 3 kb *Xho I-Xho I* fragment was removed to make plasmid pBPF22XE containing a 7.2 kb genomic fragment. A cMyc epitope tag was added at the N-terminus using overlapping PCR. The resulting plasmid has a *Sal I* site introduced 6 bp 5′ to the start codon and encodes the entire PF22 protein, with the first two amino acids duplicated on either side of a single copy of the Myc epitope (underlined): NH_2-MDEQKISEEDLMDEHNVHH…. The resulting plasmid, pBMyc22, was co-transformed into *pf22arg7* to generate strain *MycPF22*. The apparent size of this tagged protein in all transformants examined (60 kDa) is smaller than the predicted size of 72 kDa, for undetermined reasons. To identify the mutation in *pf22*, a library of 7.2 kb *Xho I-Eco RI* fragments was generated from *pf22* genomic DNA and the insert of a plasmid containing the mutant gene, pBpf22mut, was sequenced. The sequence of the wild type gene and predicted translation product are available under Genbank accession HQ424432. Pairwise alignment and dot matrix comparison of *Chlamydomonas* (AEC04845) and human (XP_849159) protein sequences was generated by BLASTp 2.2.25+[57] with default parameters. Multiple alignment with MUSCLE[58] and unrooted tree construction (neighbor joining method with Kimura parameters) were generated by SeaView 4.2.12[59].

Immunoprecipitation and immunoblot analysis of *Chlamydomonas* proteins

Samples were prepared from whole cells or cell fractions as previously described[32]. Mouse monoclonal anti-ODA-HCβ (C11.6) anti-ODA-IC1 (C1.1), anti-ODA-IC2 (C11.4)[60], anti-ODA-HCγ (12γB)[61], rabbit polyclonals anti-ODA-HCα (B3B)[31], anti-IDA-IC140[62], anti-IDA-HC9[20], and anti-IDA-HC5[63] have been previously described. Anti-HA epitope HA7 (Sigma), anti-cMYC 9E10 (Santa Cruz), and rat monoclonal anti-HA epitope 3F10 (Roche) are commercially available. Blotted proteins were detected using HRP-conjugated secondary antibodies using Supersignal West Dura substrate (Thermo Scientific). Band density of digitized film images was determined using ImageJ software.

Human *DNAAF3* mutation identification

All 12 coding exons of *DNAAF3* were amplified from genomic DNA (primer sequences available on request). Sequence alignments were made using Sequencher software to identify variants and their likely effects were assessed using Polyphen-2 and SIFT. Two restriction digestion tests were also used: BstUI digest of the PCR product of UCL89 exon 3 and MwoI digest of the PCR product of UCL71 exon 5 (for primer sequences, see Supplementary table 3). Polymorphism databases used were dbSNP (http://www.ncbi.nlm.nih.gov/projects/SNP/), 1000 Genomes Project (http://www.1000genomes.org/) and NHLBI-ESP (http://evs.gs.washington.edu/EVS/).

Immunofluorescence analysis

Respiratory epithelial cells were obtained by nasal-brush biopsy (Engelbrecht Medicine and Laboratory Technology, Germany) and suspended in cell-culture medium. Samples were spread onto glass slides, air dried, and stored at −80°C until use. Cells were treated with 4% paraformaldehyde, 0.2% Triton X-100, and 1% skim milk prior to incubation with primary (at least 3 hours at room temperature or over night at 4°C) and secondary antibodies (30 min at room temperature). Appropriate controls were performed without the primary antibodies. Rabbit polyclonal anti-DNAH5, anti-DNALI1 and anti-DNAH9, and mouse monoclonal anti-DNAH5, anti-DNALI1 and anti-DNAI2 were described previously[17,20,40,64]. Mouse monoclonal anti-acetylated α-tubulin antibodies were obtained from Sigma (Taufkirchen, Germany), rabbit polyclonal anti-α/β-tubulin from Cell Signaling Technology (USA). Highly cross-adsorbed secondary antibodies (Alexa Fluor 488, Alexa Fluor 546) were obtained from Molecular Probes (Invitrogen). DNA was stained with Hoechst 33342 (Sigma). Confocal images were taken on a Zeiss LSM 510 i-UV. Apotome-images were taken with a Zeiss Apotome Axiovert 200 and processed with AxioVision 4.7.2.

Transmission electron microscopy

Human nasal biopsies taken from the middle turbinate were fixed in 2.5% glutaraldehyde in 0.1M sodium cacodylate buffer at 4°C, washed overnight and postfixed in 1% osmium tetroxide. After dehydration, the samples were embedded in epoxy resin. Thin sections stained with Reynold's lead citrate were imaged with a Philips CM10 electron microscope. Zebrafish were analysed as described previously[65].

Morpholino oligonucleotide knockdown and in situ hybridization in zebrafish

Antisense morpholino oligonucleotides (Gene Tools) were designed against the zebrafish *dnaaf3* gene (XM_001920983) to target the exon 3 splice donor site (*dnaaf3* MO ex3), the 5'UTR, and the exon 8 splice donor site (*dnaaf3* MO ex8). Morpholinos (2-8 ng) were injected into embryos at the 1-2-cell stage and incubated at 28.5 °C. The effective dose was defined as the morpholino concentration that resulted in the least dead fish and most fish with phenotypes. Morpholino specificity was confirmed by RT-PCR. RNA was extracted at 48 hpf using TRIzol (Invitrogen). First-strand cDNA was synthesized using random nanomers (Sigma-Aldrich) and Omniscript transcriptase (QIAGEN). Standard PCR was carried out using primers in exons 2 and 5 of *dnaaf3* for the exon 3 splice site, in exons 7 and 10 for the exon 8 splice site. Amplification of *gapdh* was used as a normalizing control. In situ hybridizations on whole-mounted embryos were carried out as described previously[66] using a *cmlc2* probe[67] and a 691 bp probe spanning the 5′ end of the *dnaaf3* transcript, amplified with primers in the 5′ UTR and exon 5 (for primer sequences, see Supplementary table 3). Embryos were dechorinated and fixed in 100% methanol overnight at −20°C. After rehydration, embryos were washed several times in PBST (0.5% Triton X-100/PBS) then blocked in 5% BSA for 1 hour. The RNA antisense probe was labelled using a digoxigenin RNA labelling kit (Roche). High speed (500fps) video sequences of zebrafish cilia were captured using a MotionPro X4 camera (Lake Image Systems UK) on an inverted Nikon Diaphot microscope, with stored sequences replayed in slow motion where necessary using a Midas 2.0 player (Xcitex).

Reference List

1. Coren ME, Meeks M, Morrison I, Buchdahl RM, Bush A. Primary ciliary dyskinesia: age at diagnosis and symptom history. Acta Paediatr. 2002; 91:667–669. [PubMed: 12162599]
2. Bush A, Hogg C, Mitchison HM, Nisbet M, Wilson R. Update in primary ciliary dyskinesia. Clin. Pulm. Med. 2009; 16:219–225.
3. Bush A. Congenital heart disease in primary ciliary dyskinesia. Pediatr. Cardiol. 1998; 19:191. [PubMed: 9565518]
4. Kennedy MP, et al. Congenital heart disease and other heterotaxic defects in a large cohort of patients with primary ciliary dyskinesia. Circulation. 2007; 115:2814–2821. [PubMed: 17515466]
5. Tan SY, et al. Heterotaxy and complex structural heart defects in a mutant mouse model of primary ciliary dyskinesia. J Clin. Invest. 2007; 117:3742–3752. [PubMed: 18037990]
6. Barbato A, et al. Primary ciliary dyskinesia: a consensus statement on diagnostic and treatment approaches in children. Eur. Respir. J. 2009; 34:1264–1276. [PubMed: 19948909]
7. Ibañez-Tallon I, et al. Dysfunction of axonemal dynein heavy chain Mdnah5 inhibits ependymal flow and reveals a novel mechanism for hydrocephalus formation. Hum. Mol. Genet. 2004; 13:2133–2141. [PubMed: 15269178]
8. Kosaki K, et al. Absent inner dynein arms in a fetus with familial hydrocephalus-situs abnormality. Am. J. Med. Genet. A. 2004; 129A:308–311. [PubMed: 15326634]
9. Yang P, et al. Radial spoke proteins of Chlamydomonas flagella. J. Cell Sci. 2006; 119:1165–1174. [PubMed: 16507594]
10. Castleman VH, et al. Mutations in radial spoke head protein genes RSPH9 and RSPH4A cause primary ciliary dyskinesia with central-microtubular-pair abnormalities. Am. J. Hum. Genet. 2009; 84:197–209. [PubMed: 19200523]
11. Heuser T, Raytchev M, Krell J, Porter ME, Nicastro D. The dynein regulatory complex is the nexin link and a major regulatory node in cilia and flagella. J. Cell Biol. 2009; 187:921–933. [PubMed: 20008568]

12. Papon JF, et al. A 20-year experience of electron microscopy in the diagnosis of primary ciliary dyskinesia. Eur. Respir. J. 2010; 35:1057–1063. [PubMed: 19840971]
13. El ZL, Omran H, Bouvagnet P. Lateralization defects and ciliary dyskinesia: lessons from algae. Trends Genet. 2003; 19:162–167. [PubMed: 12615011]
14. Olbrich H, et al. Mutations in DNAH5 cause primary ciliary dyskinesia and randomization of left-right and asymmetry. Nature Genet. 2002; 30:143–144. [PubMed: 11788826]
15. Bartoloni L, et al. Mutations in the DNAH11 (axonemal heavy chain dynein type 11) gene cause one form of situs inversus totalis and most likely primary ciliary dyskinesia. Proc. Natl. Acad. Sci. U. S. A. 2002; 99:10282–10286. [PubMed: 12142464]
16. Pennarun G, et al. Loss-of-function mutations in a human gene related to Chlamydomonas reinhardtii dynein IC78 result in primary ciliary dyskinesia. Am. J. Hum. Genet. 1999; 65:1508–1519. [PubMed: 10577904]
17. Loges NT, et al. DNAI2 mutations cause primary ciliary dyskinesia with defects in the outer dynein arm. Am. J Hum. Genet. 2008; 83:547–558. [PubMed: 18950741]
18. Mazor M, et al. Primary Ciliary Dyskinesia Caused by Homozygous Mutation in DNAL1, Encoding Dynein Light Chain 1. Am. J. Hum. Genet. 2011; 88:599–607. [PubMed: 21496787]
19. Duriez B, et al. A common variant in combination with a nonsense mutation in a member of the thioredoxin family causes primary ciliary dyskinesia. Proc. Natl. Acad. Sci. U. S. A. 2007; 104:3336–3341. [PubMed: 17360648]
20. Omran H, et al. Ktu/PF13 is required for cytoplasmic pre-assembly of axonemal dyneins. Nature. 2008; 456:611–616. [PubMed: 19052621]
21. Duquesnoy P, et al. Loss-of-Function Mutations in the Human Ortholog of Chlamydomonas reinhardtii ODA7 Disrupt Dynein Arm Assembly and Cause Primary Ciliary Dyskinesia. Am. J. Hum. Genet. 2009; 85:890–896. [PubMed: 19944405]
22. Loges NT, et al. Deletions and point mutations of LRRC50 cause primary ciliary dyskinesia due to dynein arm defects. Am. J. Hum. Genet. 2009; 85:883–889. [PubMed: 19944400]
23. Kamiya R. Mutations at twelve independent loci result in absence of outer dynein arms in Chylamydomonas reinhardtii. J. Cell Biol. 1988; 107:2253–2258. [PubMed: 2974040]
24. Huang B, Piperno G, Luck DJL. Paralyzed flagella mutants of Chlamydomonas reinhardtii. J. Biol. Chem. 1979; 254:3091–3099. [PubMed: 429335]
25. Piperno G, Mead K, Shestak W. The inner dynein arms I2 interact with a “dynein regulatory complex” in Chlamydomonas flagella. J. Cell Biol. 1992; 118:1455–1463. [PubMed: 1387875]
26. Piperno G, Ramanis Z. The proximal portion of Chlamydomonas flagella contains a distinct set of inner dynein arms. J. Cell Biol. 1991; 112:701–709. [PubMed: 1825211]
27. Mitchell DR, Kang Y. Identification of oda6 as a Chlamydomonas dynein mutant by rescue with the wild-type gene. J. Cell Biol. 1991; 113:835–842. [PubMed: 1673970]
28. Kamiya R. Functional diversity of axonemal dyneins as studied in Chlamydomonas mutants. Int. Rev. Cytol. 2002; 219:115–155. [PubMed: 12211628]
29. Freshour J, Yokoyama R, Mitchell DR. Chlamydomonas flagellar outer row dynein assembly protein ODA7 interacts with both outer row and I1 inner row dyneins. J Biol. Chem. 2007; 282:5404–5412. [PubMed: 17194703]
30. Hom EF, et al. A unified taxonomy for ciliary dyneins. Cytoskeleton (Hoboken.). 2011; 68:555–565. [PubMed: 21953912]
31. Fowkes ME, Mitchell DR. The role of preassembled cytoplasmic complexes in assembly of flagellar dynein subunits. Mol. Biol. Cell. 1998; 9:2337–2347. [PubMed: 9725897]
32. Ahmed NT, Gao C, Lucker BF, Cole DG, Mitchell DR. ODA16 aids axonemal outer row dynein assembly through an interaction with the intraflagellar transport machinery. J Cell Biol. 2008; 183:313–322. [PubMed: 18852297]
33. Yamamoto R, Hirono M, Kamiya R. Discrete PIH proteins function in the cytoplasmic preassembly of different subsets of axonemal dyneins. J. Cell Biol. 2010; 190:65–71. [PubMed: 20603327]
34. Ahmed NT, Mitchell DR. ODA16p, a Chlamydomonas flagellar protein needed for dynein assembly. Mol. Biol. Cell. 2005; 16:5004–5012. [PubMed: 16093345]

35. Geremek M, et al. Gene expression studies in cells from primary ciliary dyskinesia patients identify 208 potential ciliary genes. Hum. Genet. 2011; 129:283–293. [PubMed: 21136274]
36. Ross AJ, Dailey LA, Brighton LE, Devlin RB. Transcriptional profiling of mucociliary differentiation in human airway epithelial cells. Am. J. Respir. Cell Mol. Biol. 2007; 37:169–185. [PubMed: 17413031]
37. Meeks M, et al. A locus for primary ciliary dyskinesia maps to chromosome 19q. J Med. Genet. 2000; 37:241–244. [PubMed: 10745040]
38. Adzhubei IA, et al. A method and server for predicting damaging missense mutations. Nat. Methods. 2010; 7:248–249. [PubMed: 20354512]
39. Kumar P, Henikoff S, Ng PC. Predicting the effects of coding non-synonymous variants on protein function using the SIFT algorithm. Nat. Protoc. 2009; 4:1073–1081. [PubMed: 19561590]
40. Fliegauf M, et al. Mislocalization of DNAH5 and DNAH9 in respiratory cells from patients with primary ciliary dyskinesia. Am. J. Respir. Crit Care Med. 2005; 171:1343–1349. [PubMed: 15750039]
41. Kramer-Zucker AG, et al. Cilia-driven fluid flow in the zebrafish pronephros, brain and Kupffer's vesicle is required for normal organogenesis. Development. 2005; 132:1907–1921. [PubMed: 15790966]
42. VanRooijen E, et al. LRRC50, a conserved ciliary protein implicated in polycystic kidney disease. J Am. Soc. Nephrol. 2008; 19:1128–1138. [PubMed: 18385425]
43. Gao C, Wang G, Amack JD, Mitchell DR. Oda16/Wdr69 is essential for axonemal dynein assembly and ciliary motility during zebrafish embryogenesis. Dev. Dyn. 2010; 239:2190–2197. [PubMed: 20568242]
44. Lunt SC, Haynes T, Perkins BD. Zebrafish ift57, ift88, and ift172 intraflagellar transport mutants disrupt cilia but do not affect hedgehog signaling. Dev. Dyn. 2009; 238:1744–1759. [PubMed: 19517571]
45. Colantonio JR, et al. The dynein regulatory complex is required for ciliary motility and otolith biogenesis in the inner ear. Nature. 2009; 457:205–209. [PubMed: 19043402]
46. Rosenbaum JL, Moulder JE, Ringo DL. Flagellar elongation and shortening in Chlamydomonas. The use of cycloheximide and colchicine to study the synthesis and assembly of flagellar proteins. J. Cell Biol. 1969; 41:600–619. [PubMed: 5783876]
47. Zhao R, et al. Navigating the chaperone network: an integrative map of physical and genetic interactions mediated by the hsp90 chaperone. Cell. 2005; 120:715–727. [PubMed: 15766533]
48. Liu L, Srikakulam R, Winkelmann DA. Unc45 activates Hsp90-dependent folding of the myosin motor domain. J. Biol. Chem. 2008; 283:13185–13193. [PubMed: 18326487]
49. Wilkerson CG, King SM, Koutoulis A, Pazour GJ, Witman GB. The 78,000 M_r intermediate chain of Chlamydomonas outer arm dynein is a WD-repeat protein required for arm assembly. J. Cell Biol. 1995; 129:169–178. [PubMed: 7698982]
50. Mitchell DR, Brown KS. Sequence analysis of the Chlamydomonas alpha and beta dynein heavy chain genes. J. Cell Sci. 1994; 107:635–644. [PubMed: 8006077]
51. Takada S, Kamiya R. Functional reconstitution of Chlamydomonas outer dynein arms from alpha-beta and gamma subunits: requirement of a third factor. J. Cell Biol. 1994; 126:737–745. [PubMed: 8045937]
52. Fowkes, ME. Ref Type: Thesis/Dissertation. State University of New York Health Science Center; Syracuse, NY: The role of a 70 kDa intermediate chain in flagellar outer row dynein assembly. 1999.
53. Boulon S, et al. HSP90 and its R2TP/Prefoldin-like cochaperone are involved in the cytoplasmic assembly of RNA polymerase II. Mol. Cell. 2010; 39:912–924. [PubMed: 20864038]
54. Horejsi Z, et al. CK2 phospho-dependent binding of R2TP complex to TEL2 is essential for mTOR and SMG1 stability. Mol. Cell. 2010; 39:839–850. [PubMed: 20864032]
55. Sullivan-Brown J, et al. Zebrafish mutations affecting cilia motility share similar cystic phenotypes and suggest a mechanism of cyst formation that differs from pkd2 morphants. Dev. Biol. 2008; 314:261–275. [PubMed: 18178183]
56. Rymarquis LA, Handley JM, Thomas M, Stern DB. Beyond complementation. Map-based cloning in Chlamydomonas reinhardtii. Plant Physiol. 2005; 137:557–566. [PubMed: 15665247]

57. Altschul SF, et al. Gapped BLAST and PSI-BLAST: a new generation of protein database search programs. Nucleic Acids Res. 1997; 25:3389–3402. [PubMed: 9254694]

58. Edgar RC. MUSCLE: multiple sequence alignment with high accuracy and high throughput. Nucleic Acids Res. 2004; 32:1792–1797. [PubMed: 15034147]

59. Gouy M, Guindon S, Gascuel O. SeaView version 4: A multiplatform graphical user interface for sequence alignment and phylogenetic tree building. Mol. Biol Evol. 2010; 27:221–224. [PubMed: 19854763]

60. Mitchell DR, Rosenbaum JL. Protein-protein interactions in the 18S ATPase of Chlamydomonas outer dynein arms. Cell Motil. Cytoskeleton. 1986; 6:510–520. [PubMed: 2947699]

61. King SM, Otter T, Witman GB. Characterization of monoclonal antibodies against Chlamydomonas flagellar dyneins by high-resolution protein blotting. Proc. Natl. Acad. Sci. USA. 1985; 82:4717–4721. [PubMed: 3161075]

62. Yang PF, Sale WS. The M_r 140,000 intermediate chain of Chlamydomonas flagellar inner arm dynein is a WD-repeat protein implicated in dynein arm anchoring. Mol. Biol. Cell. 1998; 9:3335–3349. [PubMed: 9843573]

63. Yagi T, Uematsu K, Liu Z, Kamiya R. Identification of dyneins that localize exclusively to the proximal portion of Chlamydomonas flagella. J. Cell Sci. 2009; 122:1306–1314. [PubMed: 19351714]

64. Rashid S, et al. The murine Dnali1 gene encodes a flagellar protein that interacts with the cytoplasmic dynein heavy chain 1. Mol. Reprod. Dev. 2006; 73:784–794. [PubMed: 16496424]

65. Ferrante MI, et al. Convergent extension movements and ciliary function are mediated by ofd1, a zebrafish orthologue of the human oral-facial-digital type 1 syndrome gene. Hum. Mol. Genet. 2009; 18:289–303. [PubMed: 18971206]

66. Barth KA, Wilson SW. Expression of zebrafish nk2.2 is influenced by sonic hedgehog/vertebrate hedgehog-1 and demarcates a zone of neuronal differentiation in the embryonic forebrain. Development. 1995; 121:1755–1768. [PubMed: 7600991]

67. Yelon D, Horne SA, Stainier DY. Restricted expression of cardiac myosin genes reveals regulated aspects of heart tube assembly in zebrafish. Dev. Biol. 1999; 214:23–37. [PubMed: 10491254]

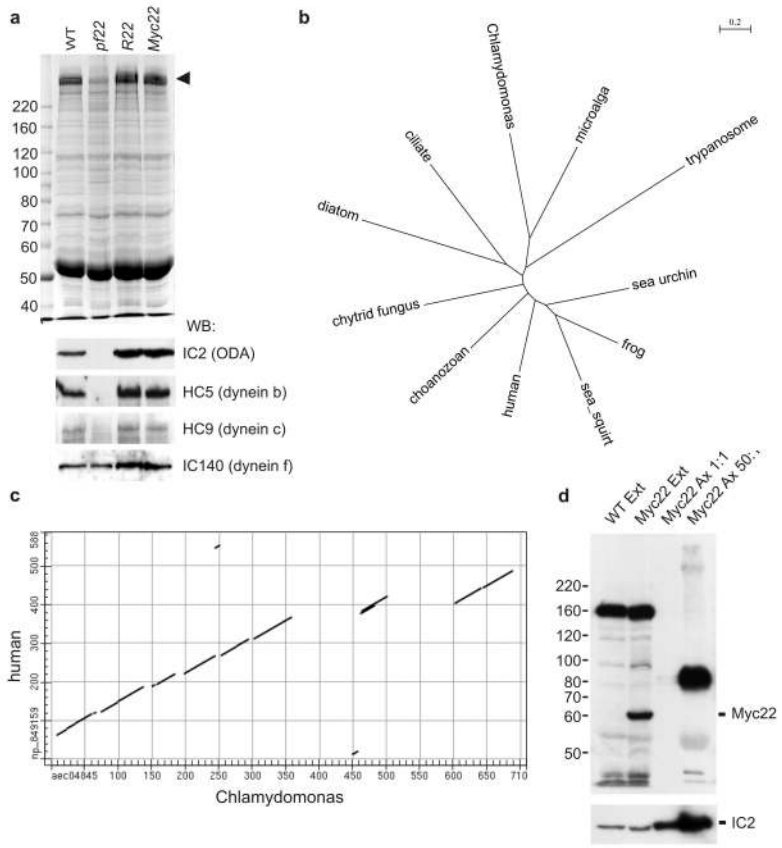

Figure 1. The *Chlamydomonas PF22* locus encodes a conserved cytoplasmic protein important for axonemal dynein assembly

(a) Demembranated flagellar axonemes from wild type, *pf22*, and the *pf22* strain transformed with untagged (*R22*) or cMyc-tagged (*Myc22*) wild type *PF22* genes probed for the presence of assembled dynein subunits. Upper panel, Coomassie-stained gel of total axonemal proteins, showing an overall reduction of high molecular weight dynein heavy chain bands in *pf22* axonemes (arrowhead). Lower panels, Western blots (WB) probed for ODA subunits (IC2) and subunits of three IDAs, showing ODAs and IDA "b" and "c" missing from pf22 axonemes, whereas IDA "f" is retained at normal levels. Assembly of all three missing dyneins is rescued by transformation with untagged or Myc-tagged gene copies. (b) Dendrogram of sequence relationships among PF22 eukaryotic orthologs shows the presence of a single orthologous sequence in each genome. (c) Dot matrix representation of sequence similarity in a pair-wise comparison of human and *Chlamydomonas* PF22 protein sequences. Similarity extends throughout both sequences except for two insertions specific to the algal protein. (d) Blots of cell fractions from *Chlamydomonas* transformed with Myc-tagged PF22 probed using anti-Myc antibody to show the relative abundance of PF22 in cytoplasmic and flagellar fractions. Upper panel: extracts from untagged (WT) and Myc-tagged (Myc22) strains show a single 60 kDa band in the transformed strain, as well as several non-specific bands. Flagellar axoneme protein loaded at a 1:1 or 50:1 stoichiometric ratio to the extract lanes does not have any detectable 60 kDa band. Lower panel: identical samples probed with anti-IC2 as a control to show the relative abundance of axonemal dynein subunits in the cytoplasmic and flagellar fractions. Numbers are size markers (kDa).

Protein sequences used in the alignments (b, c) are AEC04845 (*Chlamydomonas reinhardtii*); XP_003054829 (*Micromonas pusilla*, microalga); XP_814338 (*Trypanosoma cruzi*, trypanosome); CAK83719 (*Paramecium tetraurelia*, ciliate); ACI64850 (*Thalassiosira pseudonana*, diatom); EGF76589 (*Batrachochytrium dendrobatidis*, chytrid fungus); EGD81026 (*Salpingoeca* sp., choanozoan); NP_849159 (*Homo sapiens*, human); XP_002130641 (*Ciona intestinalis*, sea squirt); AAI08526 (*Xenopus laevis*, frog); XP_785142 (*Strongylocentrotus purpuratus*, sea urchin).

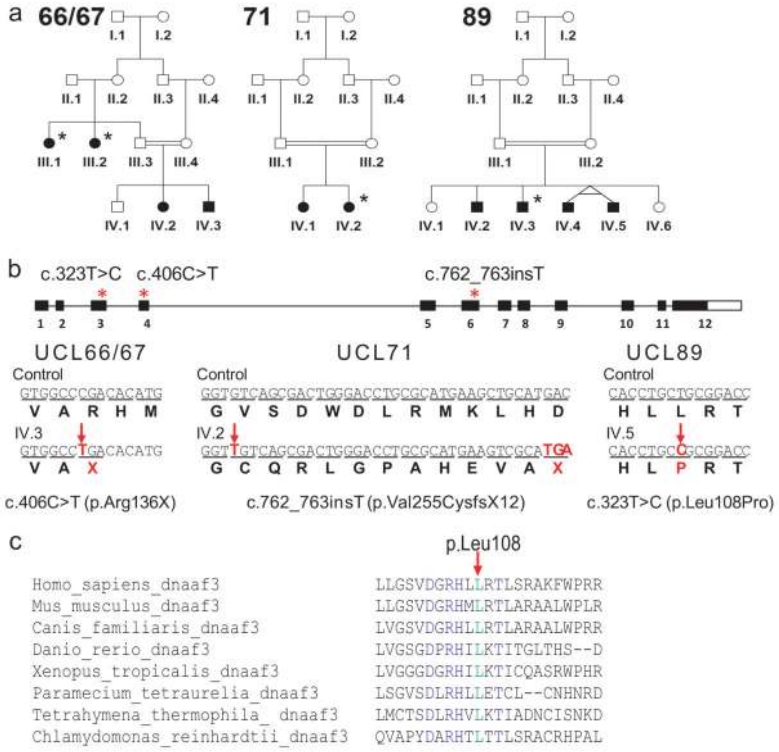

Figure 2. Identification of *DNAAF3* mutations in PCD patients with dynein assembly defects

(a) Pedigrees of three families found to carry *DNAAF3* mutations are shown. The individuals in generations I and II in each family are inferred to indicate consanguineous unions. Filled symbols indicate individuals with PCD, those with situs inversus denoted by an asterisk, and a double horizontal line represents a consanguineous marriage. UCL89 has two affected monozygous twins. (b) Sequence chromatograms for control individuals (top panels) and representative affected individuals from the families (bottom panels), show mutations in the DNA (arrows) and consequences for the protein, with the location of each mutation shown within the gene (bottom). (c) An extract of a multiple species alignment of DNAAF3/PF22 proteins is shown with the position of the highly conserved p.Leu108 residue indicated by a red arrow. Protein sequences used for the multispecies alignment are NP_849159 (*Homo sapiens*); NP_001028720 (*Mus musculus*); XP_541416 (*Canis familiaris*, dog); XP_001921018 (*Danio rerio*, zebrafish); XP_002938320 (*Xenopus tropicalis*); CAK83719 (*Paramecium tetrauralia*) and XP_001025714 (*Tetrahymena thermophila*). The *Chlamydomonas reinhardtii* protein sequence is newly reported here.

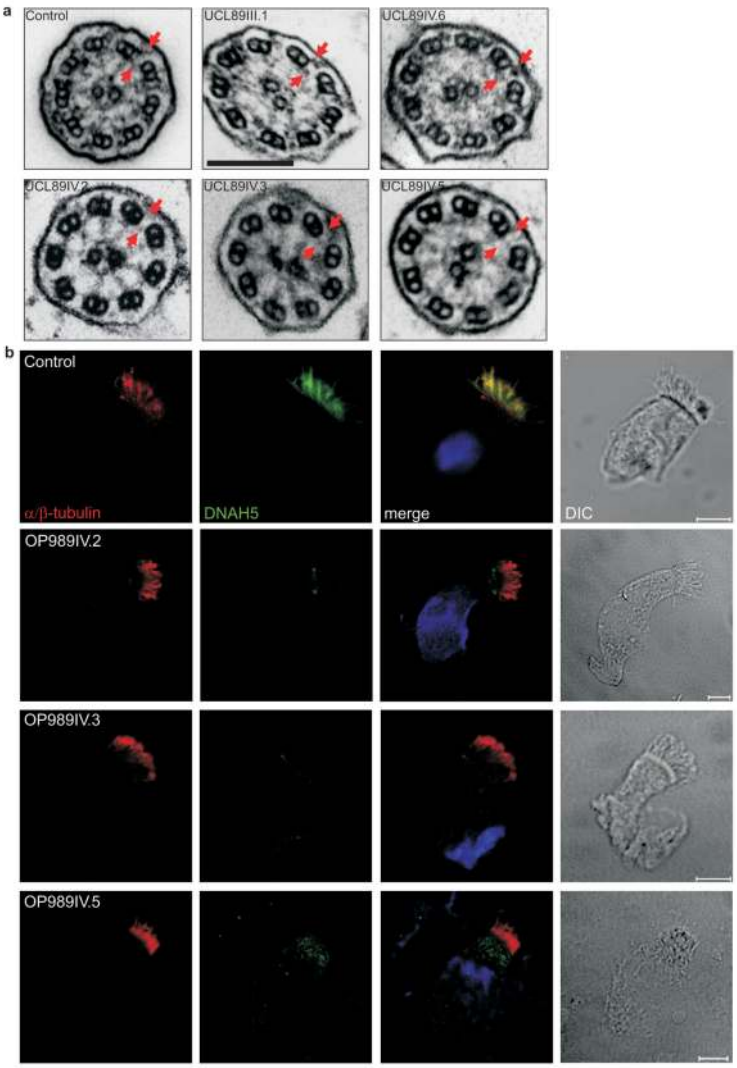

Figure 3. Absence of outer dynein arms in respiratory epithelial cell cilia of PCD patients carrying *DNAAF3* mutations

(a) Transmission electron microscopy of representative cilia cross sections in family UCL89 showing loss of both outer and inner dynein arms in affected individuals. Top row, cross sections of cilia from a control and two unaffected individuals from UCL89: III.1 (unaffected father) and IV.6 (unaffected sibling). Bottom row, cross sections of cilia from three affected siblings: IV.2, IV.3 and IV.5. The outer and inner dynein arms are indicated by red arrows. Scale bar, 0.2 um. (b) Cells double-labeled for anti-alpha/beta-tubulin to label the cilia axoneme (red) and DNAH5 (green) show that both proteins colocalize along the entire cilia in cells from the unaffected control, but DNAH5 does not appear in the cilia of any of the three affected individuals IV.2, IV.3 or IV.5, showing that DNAAF3 is necessary for outer row dynein assembly. Reduced amounts of DNAH5 label appear in the apical cytoplasm in some DNAAF3 patient cells (IV.5), suggesting that some outer row dynein proteins are present in a form that cannot assemble into cilia. Nuclei are stained with Hoechst 33342. Scale bar, 5 um.

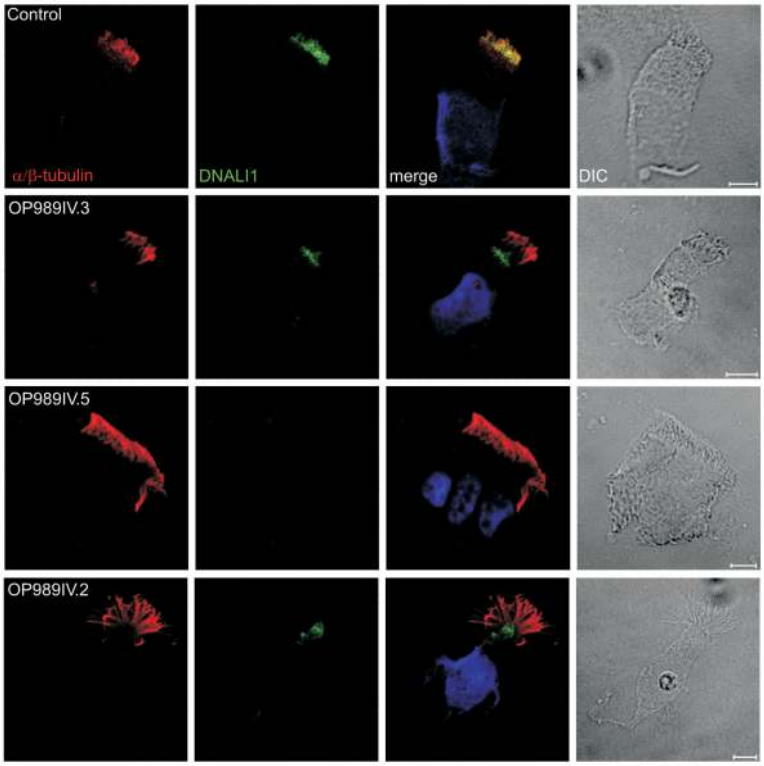

Figure 4. Absence of inner row dynein subunit DNALI1 in respiratory epithelial cell cilia of PCD patients carrying *DNAAF3* mutations

Cells double-labeled for anti-alpha/beta tubulin to label the cilia axoneme (red) and DNALI1 (green) show that both proteins colocalize along the axoneme of cilia in cells from an unaffected control, but DNALI1 is absent from the cilia of the three affected individuals IV.2, IV.3 and IV.5, demonstrating the disruption of inner dynein arm assembly in airway cilia of these patients. Nuclei are stained with Hoechst 33342. Scale bar, 5 um.

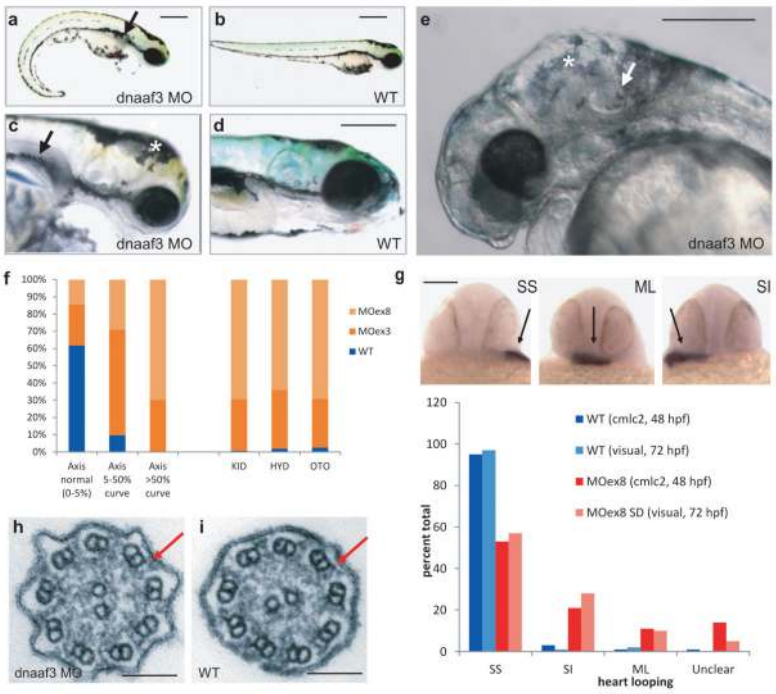

Figure 5. Morpholino knockdown of *dnaaf3* in zebrafish embryos results in axis curvature defects, kidney cysts, hydrocephalus, perturbed otolith development and laterality defects

(a-e) Representative images of phenotypes of *dnaaf3* MO-injected zebrafish embryos at 72 hours post fertilization (hpf). Morphant fish display a curly-tail phenotype compared to an unaffected sibling (a, b), develop pronephric cysts (a-d, black arrows) and hydrocephalus (c-e, white asterisks). (e) An example of a *dnaaf3* MO-injected zebrafish embryo displaying hydrocephalus (white asterisk) and an abnormal number (three) of inner-ear otoliths (white arrow). (f) Graph showing the percentage of embryos injected with *dnaaf3* MO ex3 or *dnaaf3* MO ex8 displaying the defects shown in a-e, compared to wildtype (302-315 embryos per group). Axis curvature was scored visually as normal (0-5% curl of the tail), mild with a slight curved or bent tail (5-50% curling of the tail) or severe (over 50% curling of the tail, sometimes curled over itself). The occurrence of pronephric cysts (KID), hydrocephalus (HYD) and abnormal otolith numbers (OTO) is also shown. The *dnaaf3* morphant embryos had left-right axis determination defects visualized via whole-mount in situ hybridization for *cmlc2* at 48 hpf (g, upper panel). (g, lower panel) Graph of the proportion of these phenotypes, comparing 48 hpf *cmlc2* in situ results (N=144) with visual scoring at 72 hpf of heart looping (N=315). SS, *situs solitus;* SI, *situs inversus*; ML, bilateral expression with the heart positioned along the midline; Unclear, heart position undeterminable. (h, i) Transmission electron micrographs of olfactory placode cilia cross-sections show reduction and loss of dynein arms (red arrows) in morphants compared to wildtype siblings. Scale bars = 500 μm (a, b), 200 μm (c-e, g), or 100 nm (h, i).

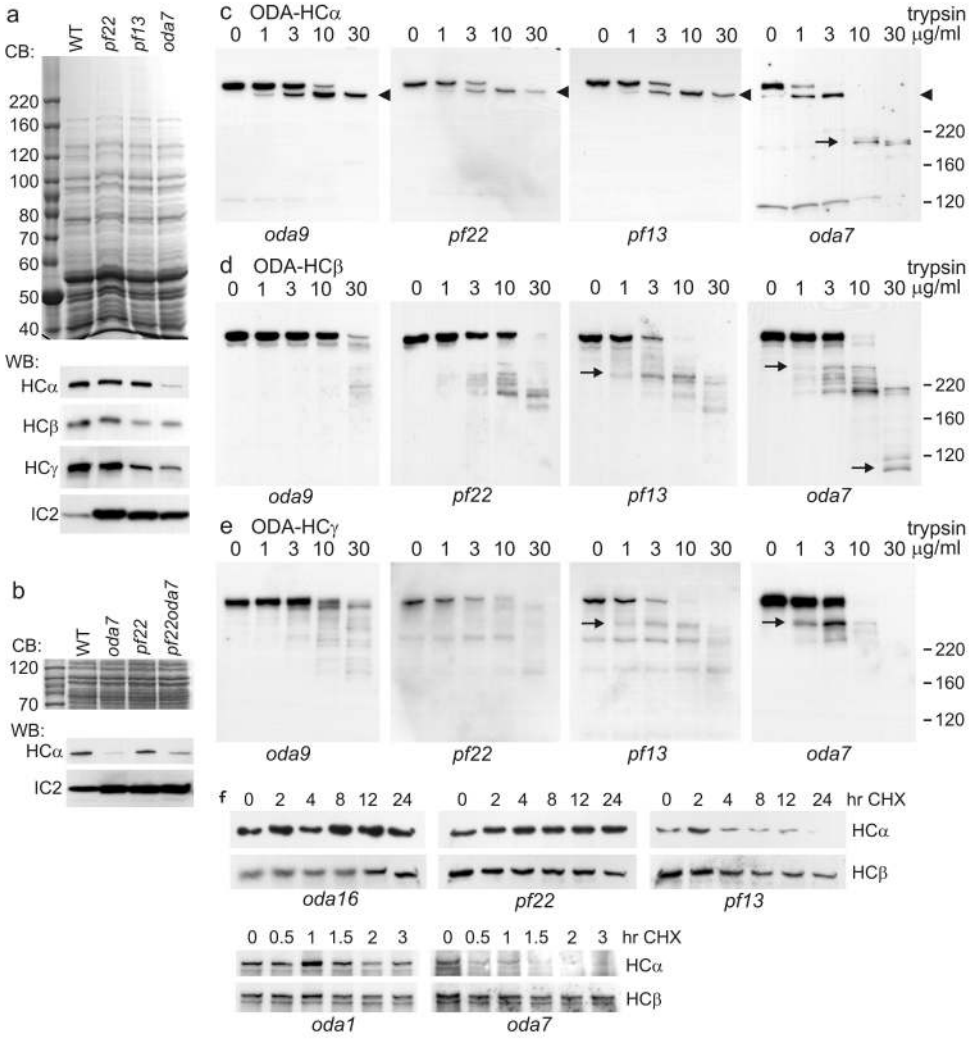

Figure 6. Altered ODA subunit abundance in the *Chlamydomonas pf22* mutant cytoplasm

(a) Cytoplasmic abundance of ODA subunits that fail to assemble in *pf22* flagella. Upper panel, stained gel shows equal loading of cytoplasmic extracts from wild type and assembly mutant strains. Lower panels, blots probed with antibodies to four ODA subunits. IC2 has an abnormally increased abundance in all three mutant strains. Dynein heavy chains appear at near-normal levels in *pf22*, but HCα is reduced in *oda7*, and both HCβ and HCγ are reduced in *oda7* and in *pf13*. (b) Comparison of HCα and IC2 cytoplasmic abundance in single mutants *pf22* and *oda7* and in a double mutant *pf22oda7* strain. HCα abundance is intermediate in the double mutant. CB, portion of Coomassie blue stained gel showing equal protein loads. (c-e) Proteolytic sensitivity of outer dynein arm heavy chains in the cytoplasm of *Chlamydomonas* assembly mutants. Extracts treated for 5 min with the indicated concentrations of trypsin were blotted for HCα (c), HCβ (d) or HCγ (e). Extracts from *oda9*, which does not alter heavy chain abundance, were used as controls. (c) Altered sensitivity of HCα is only seen in the *oda7* cytoplasm, as evidenced by rapid loss of a high molecular weight band (arrowhead) and the appearance of a new band (arrow). One non-specific band appears only on the *oda7* blot due to the 10-fold longer exposure time required to visualize

HCα in this strain. (d-e) HCβ and HCγ show altered proteolytic patterns in both *oda7* and *pf13* cytoplasm, but not in *pf22* cytoplasm. Arrows indicate bands that only appear in strains with increased heavy chain protease sensitivity. (f) Cytoplasmic heavy chain turnover tested by treating cells with cycloheximide (CHX) for the indicated number of hours. Whole cell samples were probed for outer dynein arm heavy chains HCα and HCβ. Control strains *oda1* and *oda16* have normal cytoplasmic assembly of dynein complexes (see text for details). The reductions in HCβ abundance in *pf22* and *pf13* (a,b) correlate with reduced protein half-lives (c-e). The half life of HCα is also shorter in the *pf13* cytoplasm, but unaffected in *pf22*. The greatly reduced abundance of HCα in *oda7* (a,b) correlates with a half-life reduced to less than 3 hr (f). The size of standards (kDa) is shown next to the stained gel in (a) and to the right of each *oda7* panel in (c-e).

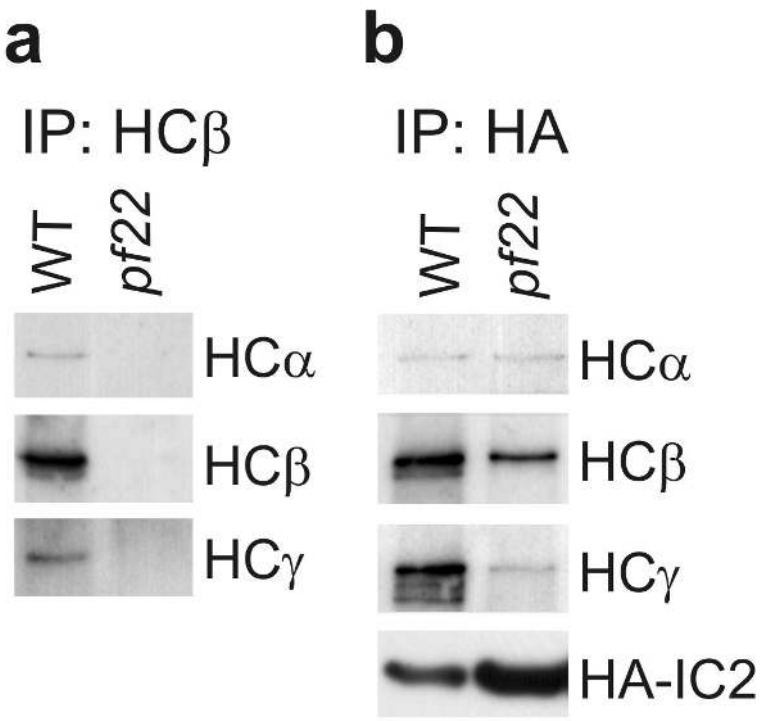

Figure 7. The *Chlamydomonas pf22* mutant fails to correctly assemble outer dynein arms in the cytoplasm

Immunoprecipitation was used to test for formation of dynein complexes in the *pf22* cytoplasm. (a) Immunoprecipitates produced with anti-HCβ monoclonal antibody were probed with antibodies to three outer row dynein subunits. All three co-precipitate from wild type cytoplasm, but the antibody failed to bind its antigen in the *pf22* extract. (b) Immunoprecipitates produced with anti-HA epitope monoclonal antibody from extracts of cells expressing HA-IC2 were probed with anti-HA and chain-specific antibodies. All three heavy chains co-precipitate with IC2 from wild type extract, and reduced amounts co-precipitate from *pf22* extract.

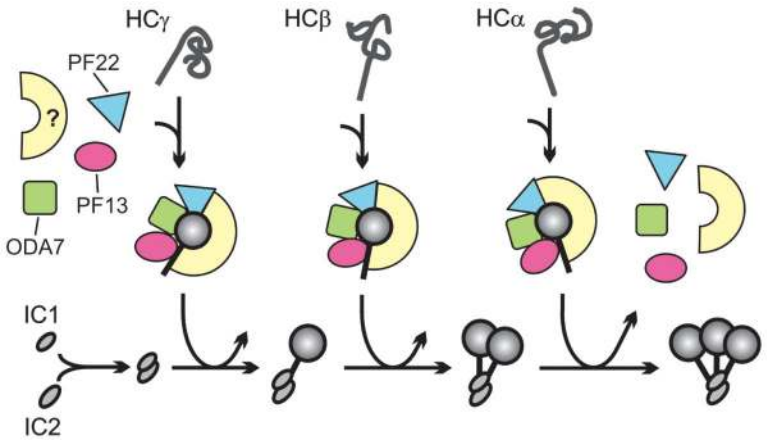

Figure 8. Hypothesized pathway of cytoplasmic assembly of axonemal outer row dynein

The three heavy chains present in *Chlamydomonas* outer dynein arms appear to require the action of ODA7 and PF13 for proper folding of their head domains, and all three assembly factors for their stability. These assembly factors may also be important for later steps in which heavy chains associate with intermediate chains. We hypothesize that these assembly factors work with a chaperone complex (labeled with "?"). In the absence of PF22, an epitope on the tail of HCβ is inaccessible; therefore PF22 may be required for dissociation of the chaperone complex at the completion of assembly. Order of addition of the three heavy chains (only two of which have orthologs in vertebrates) is speculative, but consistent with assembly defects observed previously in the absence of individual heavy chains.